

Suppression of Baroclinic Eddies by Strong Jets

OR HADAS^a AND YOHAI KASPI^a

^a *Department of Earth and Planetary Sciences, Weizmann Institute of Science, Rehovot, Israel*

(Manuscript received 25 September 2020, in final form 21 April 2021)

ABSTRACT: The midlatitude storm tracks are among the most prominent features of extratropical climate. Despite the theoretical expectation, based on baroclinic instability theory, that baroclinic eddies strengthen with jet intensification, there is evidence that this relation breaks when the jet is intense. The most well-known case is the Pacific midwinter minimum in storm-track activity, where eddy activity is diminished in winter compared to fall and spring despite the jet being the strongest in winter. To isolate the effect of jet strength on storm activity, we conduct a series of idealized GCM experiments systematically varying jet intensity. The simulations are analyzed using Lagrangian tracking to understand the response from a single-eddy perspective. The Lagrangian analysis shows that while the response of upper-level eddies is dominated by a reduction in the amount of tracked features, the lower-level eddies' response is also affected by a reduction in their lifetime. Analyzing the jet strength effect on the pairing between the upper- and lower-level eddies, we find that the jet intensification increases the relative speed of the upper-level eddies, breaking the baroclinic wave structure and limiting its growth. We show that the Lagrangian response correlates with a shift in the midlatitude spectrum to lower wavenumbers. This shift settles these results with linear baroclinic instability theory, as under the stronger jet conditions synoptic-scale eddies are predicted to have a suboptimal growth rate. These results can explain the midwinter suppression of storm activity over the Pacific and the difference from the Atlantic response.

KEYWORDS: Lagrangian circulation/transport; Jets; Storm tracks; Baroclinic models; General circulation models

1. Introduction

The dynamics of the midlatitude climate are dominated by synoptic-scale eddies, which are generated mainly by baroclinic processes. In a climatological picture, these systems form the “storm track,” which carries the bulk of the transport of momentum, heat, and moisture in the extratropics and therefore plays a vital role in Earth's climate. The fundamental theoretical understanding of the mechanisms controlling the characteristics of the storm tracks, and their relation to the general circulation, relies largely on linear baroclinic instability theory, first described by Charney (1947) and Eady (1949). A direct prediction of these models, and many of the succeeding models (e.g., Phillips 1954; Pedlosky 1970), is that the baroclinic wave growth rate and, as a result, statistical quantities such as the eddy kinetic energy (EKE), increase with baroclinicity. Indeed, midlatitude cyclones are generated preferentially in regions of strong baroclinicity characterized by sharp temperature gradients and vertical wind shear, forming the storm-track entrance regions (e.g., Nakamura and Shimpo 2004; O’Gorman and Schneider 2008a; Kaspi and Schneider 2011; Wang et al. 2017). However, there are clear examples where this linearity breaks.

Nakamura (1992) describes a case that challenges the understanding of the interaction between the mean flow and eddy activity. During winter, the meridional temperature gradient increases significantly, resulting in high baroclinicity and an intense jet stream (Figs. 1a,b for the Atlantic and Pacific Ocean basins, respectively). Over the Atlantic Ocean, the increased baroclinicity correlates to increased eddy activity, as predicted by theory (Fig. 1c), and a similar response is observed over the Southern Hemisphere (SH) storm track. However, over the

Pacific Ocean, a midwinter minimum (MWM) in eddy activity is observed (Fig. 1d), despite the baroclinicity values being of the highest observed on Earth. Nakamura (1992) showed that the midwinter minimum signal is more pronounced in the variance of high-level maps (250–500 hPa), although it also appears in lower-level fields (700–850 hPa). Furthermore, he showed that while for a jet weaker than 45 m s^{-1} the baroclinic wave amplitude is positively correlated with the jet strength, as predicted by linear theory, for more intense jets, a negative correlation appears.

The minimum in eddy activity in response to intense jet streams appears not only in reanalysis data, but also in comprehensive general circulation models (GCMs), with a physical core and parameterizations (e.g., Christoph et al. 1997; Zhang and Held 1999; Lee et al. 2013). From a Lagrangian perspective, the decreased upper-level EKE reflects the properties of the individual eddies, resulting in a reduction in the number of eddies and their intensity (Penny et al. 2010). However, the lower-level eddy response shows no reduction in the number of tracked features, and the reduction in EKE was suggested to result from a suppression in the eddy lifetime (Schemm and Schneider 2018). Baroclinic conversion was found to play a vital role in the effect, and Schemm and Rivière (2019) showed that a reduction in baroclinic conversion during midwinter over the Pacific Ocean is due to changes in the vertical structure of the baroclinic waves. Most recently, Schemm et al. (2021) studied the surface cyclones' life cycle from a synoptic perspective, and found that during the Pacific midwinter cyclones originating from Kamchatka are greatly suppressed, while cyclones from the East China Sea generally intensify, and those from the Kuroshio exhibit a mixed response, leading to an overall decrease in storm activity over the Pacific.

In recent years, studies have suggested that this effect is not directly related to the local characteristics of the western

Corresponding author: Or Hadas, or.hadas@weizmann.ac.il

DOI: 10.1175/JAS-D-20-0289.1

© 2021 American Meteorological Society. For information regarding reuse of this content and general copyright information, consult the AMS Copyright Policy (www.ametsoc.org/PUBSReuseLicenses).

Brought to you by Weizmann Institute of Science Library | Unauthenticated | Downloaded 07/23/21 03:47 PM UTC

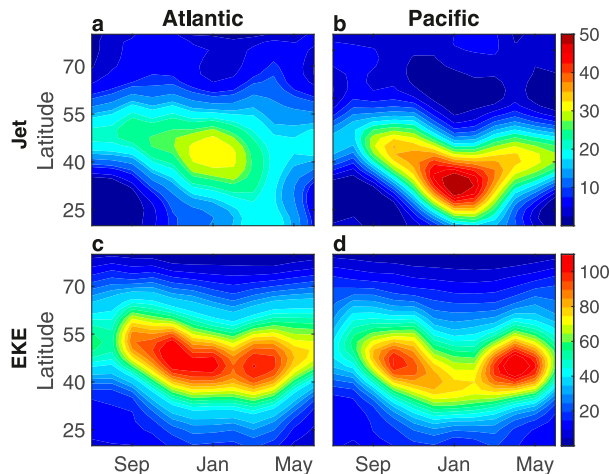


FIG. 1. (a),(b) Climatology of the mean zonal wind (m s^{-1}) as obtained from ERA-Interim at 300 hPa as a function of latitude ($^{\circ}$) and calendar month for the (a) Atlantic and (b) Pacific basins. (c),(d) As in (a) and (b), but for the eddy kinetic energy (EKE; $\text{m}^2 \text{s}^{-2}$). The climatology was made using data between the years 1980–2015. For the Atlantic, the fields are zonally averaged between longitudes 70° and 30°W , and for the Pacific between 160°E and 160°W . The EKE was calculated using a combination of a 3–10-day bandpass filter and a high-pass zonal-wavenumber 4 Butterworth filter for the meridional and zonal wind in order to capture the contribution of synoptic-scale eddies.

Pacific, but to the characteristics of the jet itself. Afargan and Kaspi (2017) showed that years with a strong zonal jet over the western Atlantic, resembling the Pacific jet, feature a prominent MWM in the Atlantic storm track as well. These years also correlate with the jet being more equatorward. The Atlantic MWM is shallower than its Pacific counterpart and maximizes during the latter part of winter (Fig. 1c). It has also been shown in idealized GCM simulations that with an adjusted Pacific-like mean zonal wind profile (Yuval and Kaspi 2016), and mean temperature for different seasons (Yuval et al. 2018), a reduction can be seen in the eddy activity during midwinter relative to shoulder seasons. Furthermore, Novak et al. (2020) showed a decrease in eddy activity during midwinter in a zonally symmetric aquaplanet GCM when the jet is strong enough.

To date, there is no one simple explanation for the observed deviations from linear baroclinic theory. Local effects, such as reduced seeding from eastern Asia (Penny et al. 2010) and stationary waves strengthening induced by the Tibetan Plateau (Park et al. 2010; Lee et al. 2013), were suggested to explain the Pacific MWM. However, the role of upstream processes has been questioned (Chang and Guo 2011), and it cannot explain the similar effect observed in the Atlantic storm track (Afargan and Kaspi 2017). Because of the importance of the midlatitude jet, mechanisms were suggested based on the jet characteristics. Particularly, the Atlantic minimum eddy activity in years marked by a stronger and more equatorward jet, as in the Pacific, provides further evidence that the jet character may be strongly related to the existence of a MWM (Yuval et al. 2018). The jet's intensity is a primary candidate for the cause of baroclinic eddy weakening. Chang (2001) suggested that

intense jets increase the group velocity of eddies, causing them to pass the high baroclinicity zones faster, which reduces their overall growth. Also emphasizing the importance of the jet strength, Nakamura and Sampe (2002) speculated that the intense jet traps the upper-level eddies, which weakens their interaction with the lower-level baroclinicity. Accounting for the jet shape, Harnik and Chang (2004) showed that linear theory could be consistent with the MWM if its meridional structure is considered, accounting for the jet's narrowing. Deng and Mak (2005) studied the effect of the horizontal structure of the jet stream, and suggested that increased baroclinicity over the Pacific could act as a generalized barotropic governor (James 1987).

In this study, a combination of an idealized GCM and Lagrangian tracking is used to investigate the effect of strong zonal jets on the activity of upper- and lower-level eddies. Using an idealized GCM for this purpose has two main advantages: First, the simplicity of the model makes the connections between atmospheric features in the system rather simple, enabling the control of the simulation characteristics without damaging its physical consistency. We take advantage of this property to control the subtropical jet by heating a zonally symmetric band around the Hadley cell's ascending branch, which strengthens the jet strength through enhancement of the Hadley circulation. Furthermore, the fact that the model is zonally symmetric simplifies the analysis and the understanding of the phenomenon. Second, the simplicity of the model allows the tracking of tens of thousands of storms, making the Lagrangian analysis very powerful, as we can produce a large database that can be used to perform complex statistical analyses, and clear multistorm composites. Using these data, we hope to understand the direct effect of strong zonal jets on baroclinic eddies, and explain the observed deviations from the linear baroclinic theory predictions.

This paper is organized as follows: The GCM simulations and their climatology, as well as the tracking algorithm, are presented in section 2. Section 3a presents an Eulerian analysis of the midlatitude eddies on a control simulation versus an enhanced jet simulation. Section 3b describes the effect of the enhanced jet on the number of storms, their mean intensity and lifetime. The jet's effect on the vertical structure of tracked vorticity features is presented in section 3c. In section 4, we show that a reduction in synoptic-scale eddy activity when the jet strength increases can be settled with linear baroclinic models if the wavenumber of the eddies is taken into account. We summarize and discuss the results in section 5.

2. Methods

In this study, a combination of idealized GCM simulations and Lagrangian tracking is used to investigate the effect of strong zonal jets on eddy activity. These tools offer several unique advantages: First, investigating the simulation from a Lagrangian perspective, using a storm-tracking algorithm, allows us to understand the storm-track response from the single-storm perspective. Second, the use of an idealized GCM allows one to produce a large database on which Lagrangian tracking can be performed, and meaningful composites can be made (Tamarin and Kaspi 2016, 2017). Third, the idealized GCM

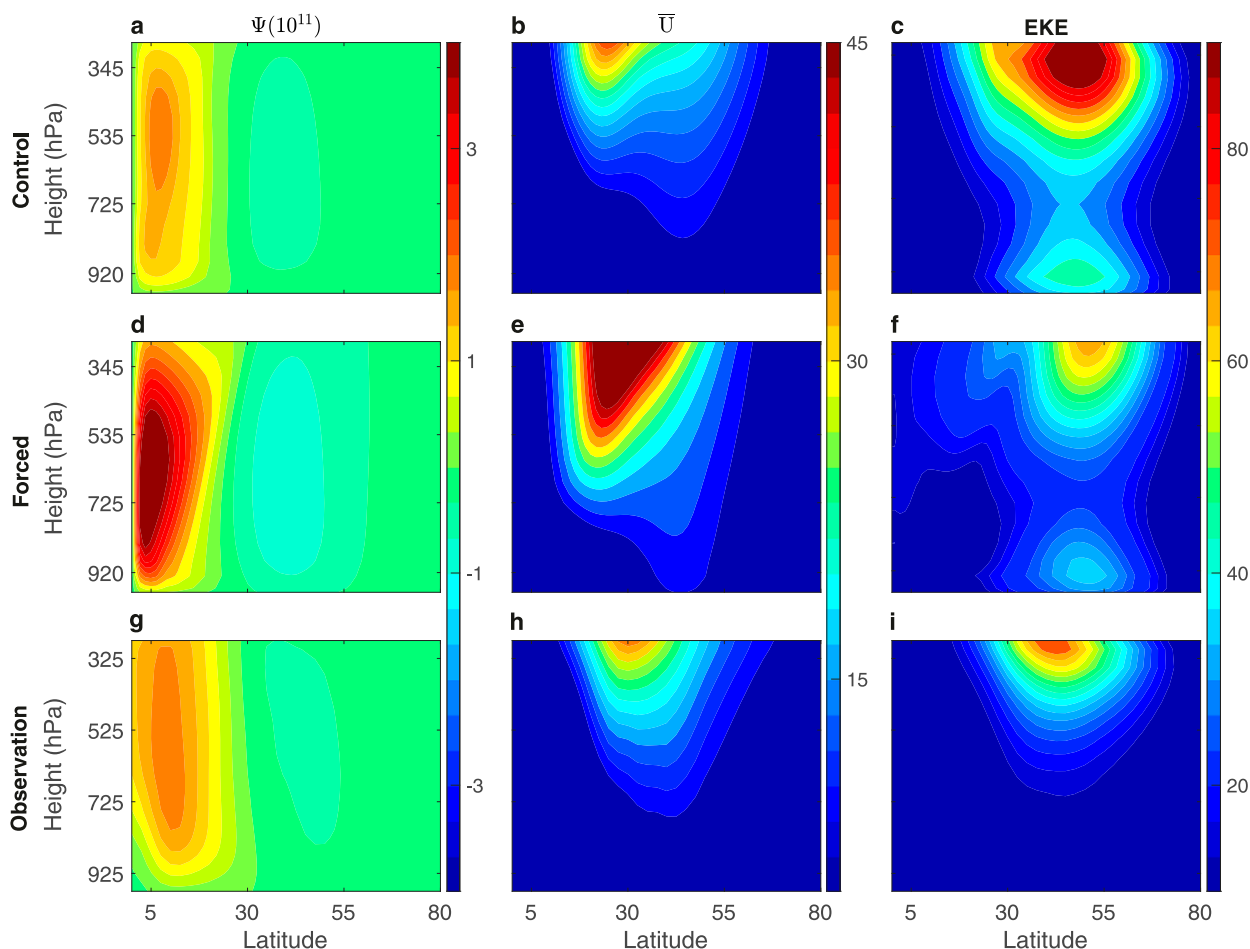


FIG. 2. Height (hPa)–latitude ($^{\circ}$) cross section of (a),(d),(g) the meridional circulation ($10^{11} \text{ kg s}^{-1}$), (b),(e),(h) zonal wind (m s^{-1}), and (c),(f),(i) EKE ($\text{m}^2 \text{ s}^{-2}$) climatology for the (top) control and (middle) forced simulations climatology, and (bottom) climatology of the Pacific Ocean during December–February made with ERA-Interim data. The GCM climatology is taken over 9000 days and averaged over the zonal direction. The GCM EKE was calculated using a high-pass zonal wavenumber 4 Butterworth filter of the zonal and meridional winds in order to capture the contribution of synoptic-scale eddies. The ERA-Interim climatology was taken as in Fig. 1, and the zonal mean was taken over the entire NH.

allows us to isolate the factors that affect the storm track and gives insight to the causality between the changes in the jet and the eddies' response. Fourth, conducting a series of GCM experiments with a gradual increase in the jet strength enables the isolation of the jet's effect on the eddy activity and the identification of different regimes of the response. Furthermore, keeping the GCM zonally symmetric simplifies the analysis and helps to understand the observed responses. The model data are compared to ERA-Interim [Dee et al. 2011; see Tamarin-Brodsky and Hadas (2019) for specifications].

a. GCM experiments

We use an idealized GCM based on the Geophysical Fluid Dynamics Laboratory (GFDL) Flexible Modeling System (FMS). This model has a spectral core, which solves the primitive hydrostatic equations for an ideal-gas atmosphere (Frierson et al. 2006; O'Gorman and Schneider 2008b). The

model is three-dimensional with spherical geometry, and we use a spectral resolution of T85, which corresponds to grid boxes of $1.4^{\circ} \times 1.4^{\circ}$ and 30 vertical levels. The incoming radiation is modeled as a perpetual equinox, with no daily or seasonal cycle. The simulation is an aquaplanet; the lower boundary is a slab ocean with a prescribed heat capacity. The surface temperature is determined by the balance between the radiation energy and the surface fluxes. Moist convection is set to relax the temperature profile to a moist adiabat, and moisture is removed through condensation and precipitation when moisture in a grid box exceeds saturation. The model does not include clouds, ice, and chemical processes. The climate produced by the model is similar to the general circulation observed on Earth (Fig. 2), and was used previously to study storm-track dynamics (e.g., Tamarin and Kaspi 2016).

To investigate the effect of enhanced midlatitude baroclinicity and intense subtropical jets on eddy activity without forcing the extratropics directly, we enhance the Hadley

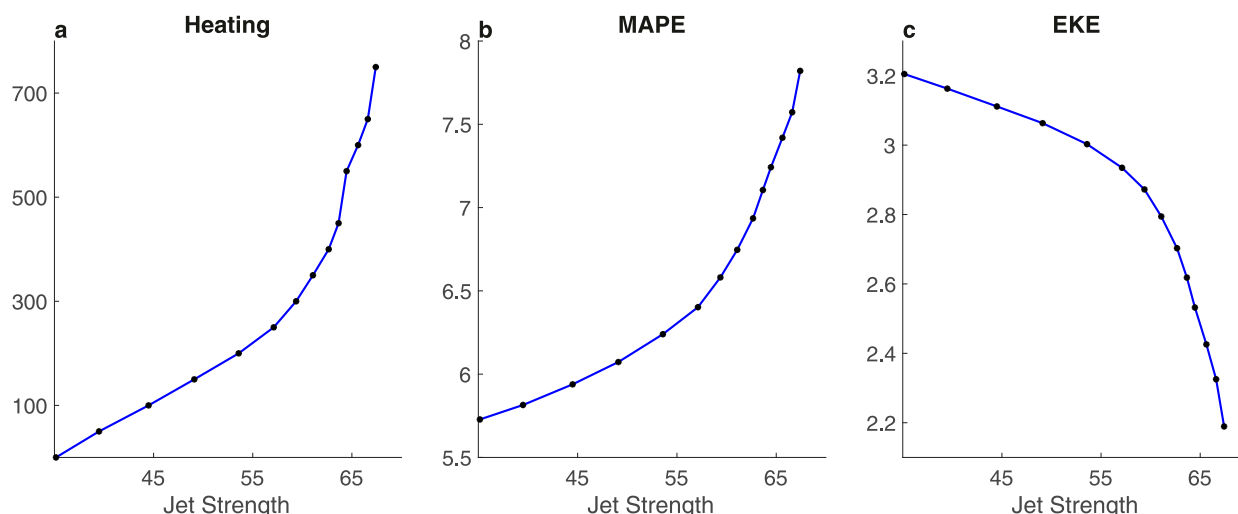


FIG. 3. Eulerian characteristics of the 14 simulations: (a) the simulation equatorial heating (W m^{-2}) vs the resulting jet strength (m s^{-1}). (b) The MAPE ($\text{J m}^{-2} \times 10^5$) as function of the simulation jet strength. (c) The vertically integrated EKE per unit area ($\text{J m}^{-2} \times 10^4$) as function of the jet strength. The MAPE was calculated as in Yuval and Kaspi (2016). The data were smoothed using a moving average to improve clarity.

circulation (and the jet) through a zonally symmetric heating of the Hadley cell ascending branch, between the equator and latitude 6° in both hemispheres. The indirect midlatitude forcing is used to avoid artifacts and direct interference of the midlatitude thermal and wind structure. We conduct a systematic set of 14 experiments with a heat flux ranging between 0 and 750 W m^{-2} , which result in jet strengths of $35\text{--}67 \text{ m s}^{-1}$ (Fig. 3a). By heating only the equatorial regions, the midlatitudes are affected only through interaction with the stronger jet (Afargan 2018). The climatology of the zonal mean meridional streamfunction, zonal flow, and EKE for the control simulation and the simulation heated by 750 W m^{-2} (the “forced simulation”) are shown in Fig. 2. Reanalysis data zonally averaged over the NH during midwinter are shown in Fig. 2 as well. The forced simulation roughly doubles the strength of the meridional circulation (Figs. 2a,d) and, as a result, the jet (Figs. 2b,e), while weakening the EKE, mostly at high levels (Figs. 2c,f). The general structure and the values in the simulations are comparable to those observed on Earth, (Figs. 2g–i). The changes in the jet and EKE for all the simulations (Figs. 3a,b) show that the jet intensification and reduction in EKE are consistent and gradual across all simulations. The mean available potential energy (MAPE) (Fig. 3c) increases with the jet intensification, implying that the reduction in EKE is not due to a decrease in the MAPE.

b. Storm tracking

A feature point-tracking algorithm (Hodges 1995; Tamarin and Kaspi 2016) is used to identify and characterize the extratropical eddies. The 850 hPa relative vorticity (defined as $\xi = \partial v/\partial x - \partial u/\partial y$, where u and v are the zonal and meridional wind and x and y are the zonal and meridional directions, respectively) is tracked to identify the surface cyclones, and the 500 and 300 hPa relative vorticity, to identify the higher-level eddies. We filter the data and smooth it to T42 resolution to

reduce noise and remove the background flow (defined as wavenumbers 0–4) to isolate the synoptic and mesoscale features. Only anomalies with relative vorticity of more than 10^{-5} s^{-1} are tracked, to account only for significant events. After identifying the anomalies, the algorithm tracks them and plots their location on the sphere and their intensity. A snapshot from the control simulation of vorticity at the different levels with the identified anomalies is shown in Fig. 4. The algorithm captures most of the anomalies, even for the high levels, where the structure appears to be much more complex. The tracks are used both for characterizing the eddy properties at the different level and to characterize baroclinic wave, realizing that each track is part of a 3D wave.

After identifying the anomalies, the algorithm tracks their evolution, and only those that appear for more than 48 h and propagate for more than 1000 km are recorded. Vorticity features whose overall movement through their lifetime is to the west, and have not passed latitude 35° (which is the climatological northward flank of the subtropical jet in the control simulation), are filtered out to exclude from our analysis tropical cyclones. Overall, about 20 000 upper- and lower-level systems were identified, which is about an order of magnitude more tracks than can be obtained over the Pacific during midwinter from ERA-Interim data.

Comparing the tracking results of geopotential height anomalies (as in Schemm and Rivière 2019) and vorticity anomalies should be done with caution. When tracking features such as the lower-level geopotential height, which are closed contours, the maximum vorticity is located on top of the geopotential height minimum. However, due to the upper-level jet, the upper-level eddies are often open contours (wave-shaped eddies), and while their minimum geopotential height is in the middle of the meanders, the maximum vorticity is on the wave tip, where the wind curvature is maximum, which is much more equatorward.

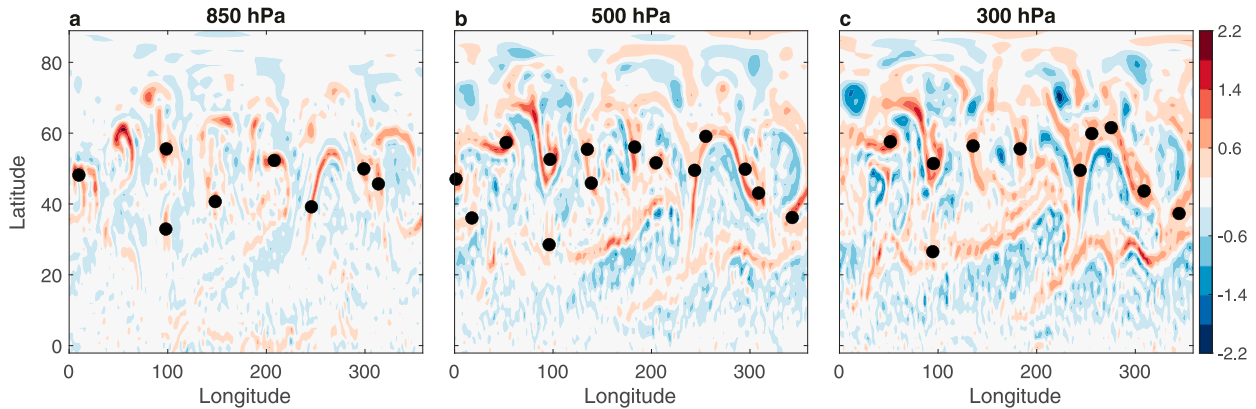


FIG. 4. Vorticity anomalies identified by the tracking algorithm (black circles) plotted on a longitude ($^{\circ}$)–latitude ($^{\circ}$) cross section of the (a) 850, (b) 500, and (c) 300 hPa vorticity (10^4 s^{-1}). The snapshots are taken from the control simulation NH.

3. Results

a. Eulerian analysis of the midlatitude eddies

Ultimately, we would like to use the Lagrangian tracking to decompose the observed change in EKE into the effect on the individual eddies. To gain some intuition for the effect of the jet on the eddies, we begin by considering the temporal evolution of vorticity anomalies at 850 and 300 hPa over the midlatitudes. In the control simulation, the eddy activity is apparent at high and low levels at latitudes 30° , 40° and 50° , with the eddies becoming stronger and more abundant at higher latitudes (Figs. 5a–c, long narrow lines). The upper- and lower-level eddies move with similar zonal speed toward the east, maintaining a westward tilt with height. According to baroclinic instability theory, this westward tilt with height (apparent as the westward shift between 300 and 850 hPa eddies in Fig. 5) plays a significant role in maintaining an optimal growth rate (Eady 1949). In the forced simulation (Figs. 5d–f), the eddies at latitude 30° and 40° are fewer and seem to have a shorter lifetime, apparent from the fewer and shorter lines of vorticity anomalies. At those latitudes, the zonal velocity of the upper-level eddies is greater than that of the lower-level eddies, and therefore, the westward-tilt structure is not maintained. At latitude 50° , the eddy activity is similar between the simulations, although the eddies in the forced simulation are fewer and have a shorter lifetime.

Overall, the reduction in eddy activity is prominent in the snapshots. The effect is more significant at lower latitudes and higher altitudes, which fits the EKE’s observed response. Moreover, the difference between upper- and lower-level eddies motivates the Lagrangian analysis on both vertical levels in order to better understand the different responses.

b. Eddy properties

To understand the mechanism that causes the EKE weakening seen in the Eulerian analysis, the effect on the eddies is studied from a Lagrangian perspective. Guided by the response observed in Fig. 5, the reduction in the EKE is decomposed into three main eddy properties. The first is the storm’s intensity: the more intense the storm is, the higher is its

contribution per unit time.¹ The second is the storm’s lifetime: the longer the storm lives, the higher is its contribution to the EKE. The third, is the number of storms passing through the storm track: more storms result in more EKE. To evaluate the above properties, we use the total number of tracked features to assess the number of eddies, the maximum vorticity of each storm as the storm’s intensity, and the time between the discovery of the anomaly and its disappearance as its lifetime (Fig. 6).

For the upper-level eddies, the number of features, their mean intensity, and their lifetime all decrease when the jet strength increases (Fig. 6, solid). The robust reduction in all eddy properties explains the intense reduction in the upper-level EKE observed in the simulation (Fig. 2f). The relative decrease in the number of storms is twice the relative reduction in the lifetime and is significantly more substantial than the relative change in intensity. Most of the reduction in the lifetime of the storms is during the growth stage (before maximum intensity), although the decay phase (after maximum intensity) also shortens (Fig. 7b). This is consistent with the significant reduction in the number of upper-level eddies and their intensity observed over the Pacific during midwinter in reanalysis data (Penny et al. 2010).

For the lower-level eddies, the decrease in the number of storms dominates the response only for very intense jets (Fig. 6a, dashed). Conversely, for less extreme jets, the reduction in lower-level EKE is also highly effected by shortening of the eddy lifetime (Fig. 6c, dashed). The reduction in lifetime is due to a shortening of the growth phase, while there is no significant reduction in the decay phase (Fig. 7a). The shortening of the growth phase is more significant than that of the decay also during midwinter over the Pacific (Schemm et al. 2021). A reduction in the eddy intensity appears mostly for very intense jets (Fig. 6b, dashed). These results are intriguing

¹ The storm area is another factor that might change with the jet intensification. We assume that the storm area is positively correlated to the storm intensity and will add a nonlinear term to the intensity contribution.

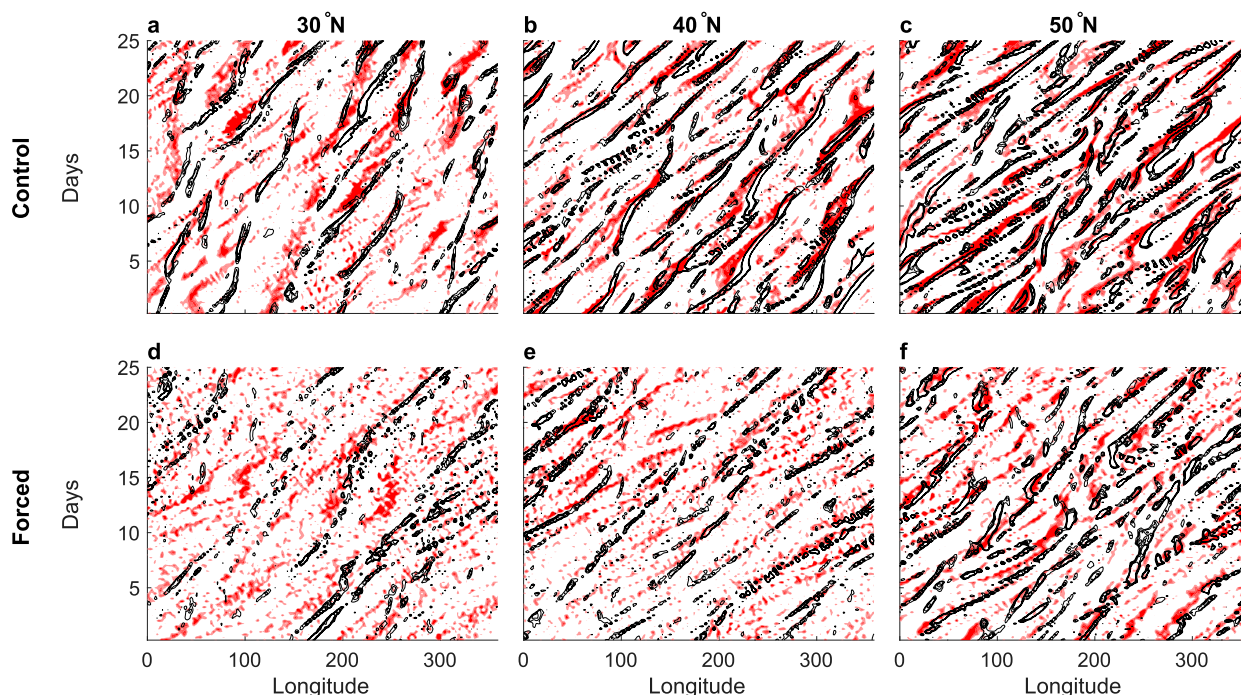


FIG. 5. Hovmöller diagram of 300 hPa (red) and 850 hPa (black contours) vorticity at latitudes of (a),(d) 30°, (b),(e) 40°, and (c),(f) 50° for the (top) control and (bottom) forced simulations as a function of longitude (°) and time (days). Eddy activity can be identified as long, narrow lines propagating to the east. The first contour and the intervals between contours are $2 \times 10^{-5} \text{ s}^{-1}$ for both high- and low-level vorticity. The vorticity field is filtered using a high-pass wavenumber 4 filter.

in light of the findings of [Schemm and Schneider \(2018\)](#), who showed, using reanalysis data, that the number of lower-level eddies increases during midwinter over the Pacific, and the reduction in EKE is due to a decrease in the eddy lifetime. The

response observed over the Pacific raises the question of whether the increase in the number of lower-level features is a general property of baroclinic eddy response to strong zonal jets or the regime of the response observed specifically over the

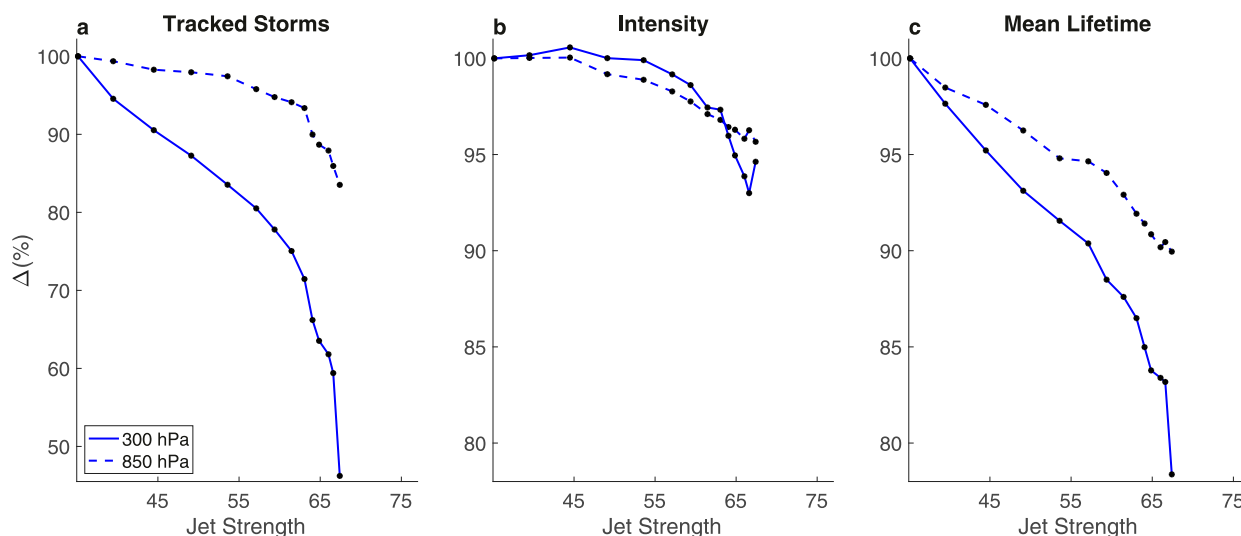


FIG. 6. The relative change (i.e., simulation value/control value) in the amount of (a) tracked features, (b) average peak eddy intensity, and (c) mean lifetime as a function of the simulation jet strength (m s^{-1}) as a consequence of the forcing for 300 hPa (solid) and 850 hPa (dashed) tracked vorticity. In the control simulation, 24 000 lower-level cyclones were tracked, with a mean maximum intensity of $5.6 \times 10^{-5} \text{ s}^{-1}$ and a mean lifetime of 6.1 days, while 25 000 upper-level eddies were tracked, with a mean maximum intensity of $7.0 \times 10^{-5} \text{ s}^{-1}$ and a mean lifetime of 4.9 days.

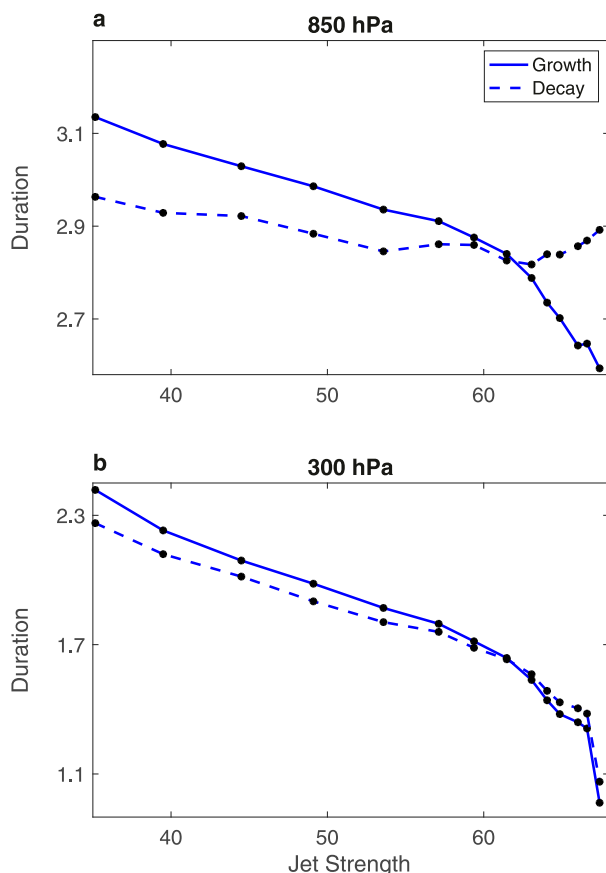


FIG. 7. The average duration (days) of the growth (solid) and decay (dashed) phases as a function of the simulation jet strength (m s^{-1}) for tracked (a) 850 and (b) 300 hPa eddies. Growth is defined as the time between discovery and maximum intensity of an eddy, and decay is defined as the time between maximum intensity and eddy disappearance.

Pacific. In light of Schemm et al. (2021), the change in the number of cyclones during midwinter appears to vary across different regions of the west Pacific, while the reduction in the growth time of cyclones is robust throughout the west Pacific. Thus while a decrease in the number of tracked features dominates the upper-level weakening, the lower-level response is highly affected by the reduction in the eddy lifetime. In addition, the upper-level eddy response is much stronger, due to the direct interaction with the jet, and consistent with the more significant reduction in the upper-level EKE.

c. Vertical structure response to intense jets

According to baroclinic instability theory, the upper- and lower-level eddies are not independent but rather a part of a three-dimensional wave. The wave's vertical structure influences the growth rate, and the maximum growth rate is achieved when the wave is westward tilted with height (Eady 1949). To understand how the eddy response, analyzed in section 3b, is translated into a response of the baroclinic wave, the effect of the intense jet on the relations between eddies at different levels is analyzed. To gain intuition on the jet effect,

we plot a snapshot of 850 and 500 hPa vorticity with the tracking data on top for the control and forced simulation (Figs. 8a and 8b, respectively). In the control simulation, most of the low-level cyclones have a corresponding upper-level positive vorticity anomaly above them. In the forced simulation, fewer features appear (consistent with the findings shown in Fig. 6), and more of them are isolated, i.e., without an upper-level companion.

To quantify these findings, we present composites of upper-level tracked features location relative to the lower-level cyclone (Figs. 8c–e). For each time step in the lower-level eddy track, all the upper-level eddies' longitudinal and latitudinal positions at that time are recorded. These maps are then sorted according to their time lag from the maximum intensity of the lower-level eddy. Maps in the same life phase are clustered together and transformed into a 2D kernel distribution. For this analysis, the threshold for detection of upper-level eddies was reduced to only existence of more than 24 h (relative to 48 h in other parts of the analysis), and the limitation on the minimum traveling distance was removed. This lower threshold was set to minimize the number of missed upper-level eddies, as we assume that having a false positive recognition around the lower-level eddies is unlikely. The kernel distributions (Figs. 8c–e) for one day before peak intensity, at the time of peak intensity, and one day after maximum intensity have a prominent peak around the center of the lower-level system, meaning that the analysis observes a correlation between the upper and lower wave. During the growth stage and at the maximum intensity, the upper-level features appear to the west of the lower-level (Fig. 8c,d), consistent with baroclinic instability theory. The primary time evolution in the 2D distribution is the propagation of the distribution to the south and east relative to the low-level system. The eastward propagation breaks the baroclinic structure, which ignites the eddy barotropic decay (Simmons and Hoskins 1978). The main difference in distribution between the two GCM simulations (Fig. 8c–e, color versus contours), is the faster eastward propagation in the forced simulation, which is even more significant if we recall that the growth phase is shorter for the forced simulation (Fig. 7). As can be gathered from the findings presented in Fig. 5, faster propagation of the upper-level eddies is apparent mostly at low latitudes, where the upper-level eddies are drifting faster under the direct effect of the very intense jet.

To better understand the temporal evolution of the eddy vertical structure and the effect of the enhanced jet on it, the position of the maximum of the distribution is plotted as a function of time in the meridional and zonal directions (Figs. 9a and 9b, respectively). The maximum intensity time step (which is used as a reference time step for the composites) is set to the average growth time of the eddies in each simulation (taken from the results of Fig. 7a) to account for the shortening of the growth phase in the forced simulation. The same general trend is observed for the control and forced simulations: the upper-level eddy begins to the west of the lower-level eddy, in agreement with the expected westward tilt with height, and then starts propagating to the southeast. About 12 h after the maximum intensity, it turns to propagate to the northeast.

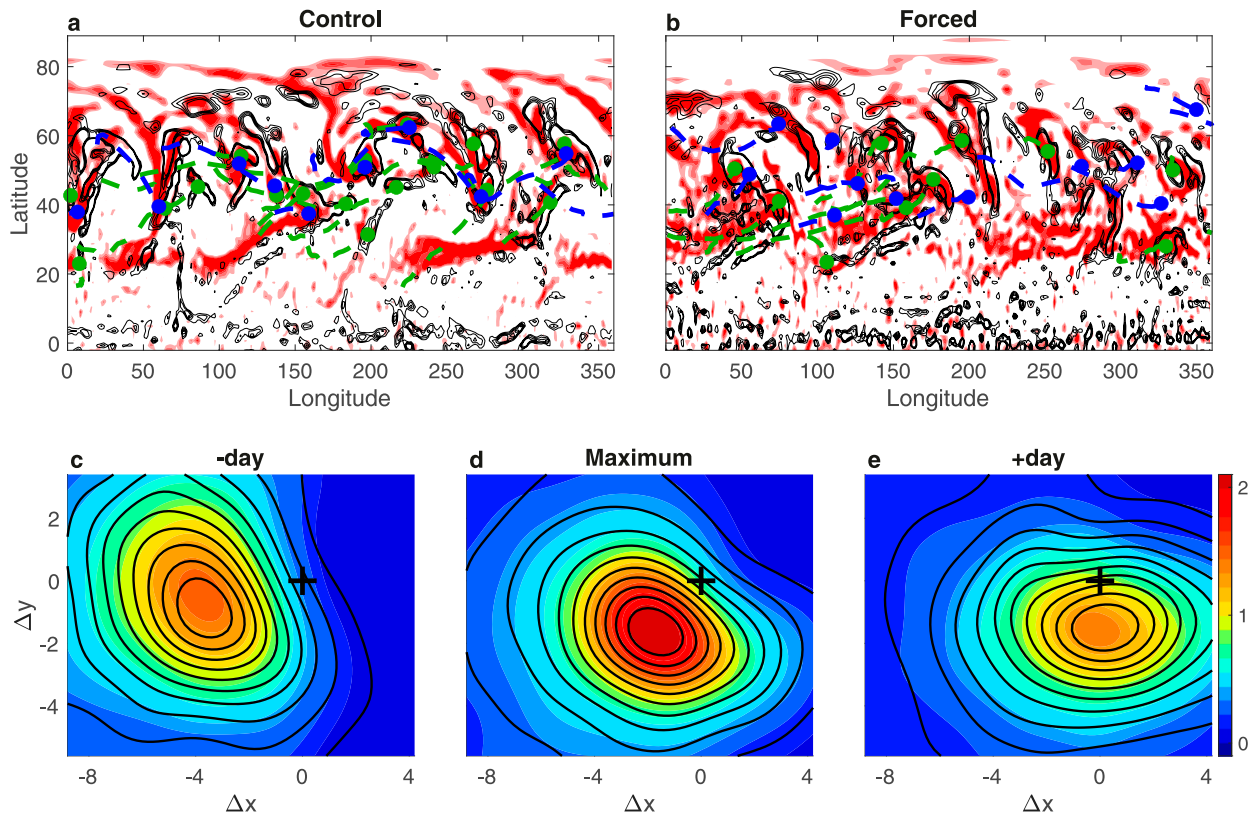


FIG. 8. Pairing of high- (500 hPa) and low- (850 hPa) level eddies. (a),(b) Snapshots of high- (red) and low-level (black contours) vorticity for the NH of the (a) control and (b) forced simulations with the high (blue dots) and low (green dots) tracks. Dashed lines in the respective colors are the tracks of the eddies from genesis to the current time step. The first contour and color and the spacing between the contours and coloring is $2 \times 10^{-5} \text{ s}^{-1}$. (c)–(e) The concentration of tracked features ($\% \text{ } ^\circ^{-2}$) at 500 hPa as a function of the relative distance ($^\circ$) from the low-level eddy center for the control (color) and forced (contours) simulations (c) a day before maximum, (d) at maximum, and (e) a day after maximum intensity. The black crosses represent the lower-level eddy center.

However, some significant differences are observed. In the zonal direction, the upper-level wave propagates faster and farther eastward relative to the lower-level eddy, which means that, according to baroclinic instability theory, the growth rate reduces more rapidly, which shortens the lifetime of the wave and decreases its maximum intensity. Indeed, calculating the relative change in propagation speed of the upper- and lower-level eddies, we find that while the lower-level eddies become faster by 15%, the upper-level eddies get faster by 31%. After maximum intensity, the upper-level wave in the forced simulation propagates more toward the pole in the meridional direction, which reduces the efficiency of baroclinic conversion (Schemm and Rivière 2019). The response in the meridional direction reported here is comparable to the one found over the Pacific in Schemm and Rivière (2019).² In the zonal direction, they found that the wave is more to the west. This discrepancy might be caused by the fact that they cluster the

entire lifetime together, which means that the more westward orientation might not be due to the change in the upper-level wave relative speed, but rather a result of how they made the composite and how the Pacific seasonality affects it.

The larger decrease in the amount and lifetime of upper-level eddies, compared to the decrease of these properties in lower-level eddies (Fig. 6) points to another significant effect of the intense jet: a reduction in the number of lower-level storms that are paired to an upper-level trough. If we consider only upper-level eddies with a center at a distance between -7° and 3° in the zonal direction and -5° and 3° in the meridional direction (the box was chosen to be big enough, so the maximum position difference will not affect the calculation), we find that 66% of the tracked lower-level eddies in the control simulation are paired with an upper-level companion (Fig. 6d). However, in the forced simulation, only 58% of the lower-level eddies are paired, a relative decrease of about 12%. The continuous response to the jet strength shows this reduction is robust and strongly dependent on the jet strength (Fig. 9d). The absence of the upper-level eddies above the lower-level wave is not straightforward in the frame of linear baroclinic instability theory, as it handles the storms as a single wave. To better

² In their research, Schemm and Rivière (2019) tracked geopotential height rather than vorticity. Therefore, only the response to the jet intensification is comparable, not the actual relative position. See section 2b.

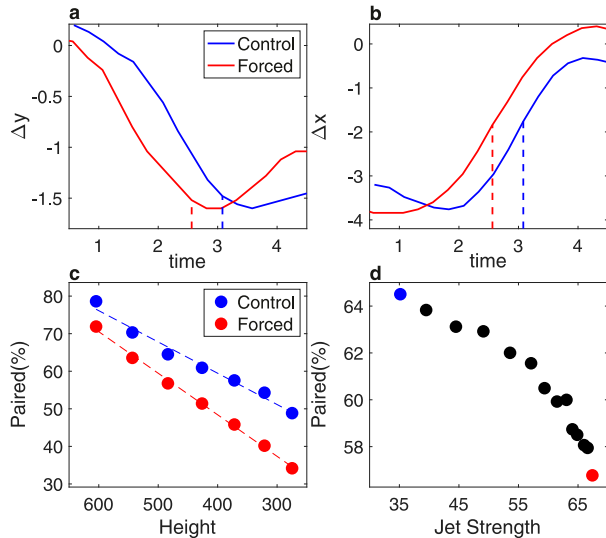


FIG. 9. (a),(b) The position of the peak in the tracked 500 hPa eddies distribution (shown in Fig. 8c–e) relative to the 850 hPa eddies in the (a) meridional and (b) zonal directions as function of time (days) from genesis. (c) The percentage of 850 hPa eddies, in their maximum intensity, that have a tracked eddy above them (“paired” eddies) at different heights for the control (blue) and forced (red) simulations. (d) The percentage of paired 850 hPa (in their maximum intensity) and 500 hPa eddies as a function of the simulation jet strength. The curves in (a) and (b) are smoothed using a moving average to improve clarity. Dashed lines in (a) and (b) are the time of maximum intensity.

interpret these results, we plot the percentage of paired eddies as a function of the height of the upper-level eddy (Fig. 9c). The pairing percentage decreases with height (which is expected as all lower-level eddies are paired with themselves), with the reduction being more rapid for the forced simulation. This can be interpreted as a change in the average vertical scale of the baroclinic waves in the model, i.e., while in the control simulation more than 50% of the waves have a top higher than 300 hPa, only 35% of the waves in the forced simulation have tops that high, meaning their vertical extent is smaller. Waves with lower vertical extent were found to be weaker and short living. This reduction in wave height strongly depends on the jet strength (Fig. 9d).

In summary, we can now translate the tracked eddies’ response to jet intensification into the baroclinic waves’ response and classify it into three different effects. The first is a reduction in the number of baroclinic waves, which correlates with the reduction in lower-level features (Fig. 6a, dashed). This effect is significant mostly for very intense jets. The second is a reduction in the eddies’ vertical scale, which explains the more significant reduction in upper-level EKE (Figs. 9c,d). The third is the break of the baroclinic structure due to the faster zonal advection (Fig. 9b) of the upper-level eddies in response to the intense jet, which explains the decrease in the eddies’ maximum intensity and lifetime (Figs. 6b,c). This process dominates the lower-level eddies’ response at median jet strengths. The three effects combine to produce the Pacific MWM-like response

observed in the Eulerian analysis and the negative correlation between jet intensity and EKE for strong jets.

4. Eddy spatial-scale shift

In section 3c three aspects of the baroclinic wave response were found to explain the reduction in EKE over the midlatitudes. In this section, we show that both the reduction in the number of baroclinic waves and the suboptimal baroclinic structure observed in the forced simulation are consistent with linear baroclinic instability theory if the wavenumber of the baroclinic wave is considered.

To understand the jet intensification effect on different scales of the midlatitude, we first consider the wavenumber–period spectra of eastward-propagating waves (Fig. 10). The control simulation spectra resembles the Earth spectra (Figs. 10a,b), both in terms of the wavelength of maximum growth and in the phase speed. A linear dispersion relation can be observed in those spectra with a cutoff wavenumber of about 4 and with most of the power above wavenumber 5. In the forced simulation (Fig. 10c), no clear cutoff wavenumber is apparent. When observing the difference between the simulations (Fig. 10d), a shift to low wavenumber is observed: while in the control simulation most of the energy is concentrated in the synoptic scale ($n > 5$), in the forced simulation there is a significant shift of the spectrum toward the planetary scale ($n < 5$). An intensification of low wavenumbers (1–3) was also found in Earth’s NH during midwinter (Park and Lee 2020). This shift implies that the energy associated with synoptic-scale baroclinic eddies is expected to decrease. Assuming the difference in wave amplitude is mainly a result of the difference in wave growth rate (Farrell and Ioannou 1994), the shift to low wavenumber fits our Lagrangian findings and can manifest in two ways: First, slower growth in these scales will make the storms more susceptible to dissipative forces, which reduce the number of baroclinic waves in the storm track. Second, the shift of the optimal wavenumber toward lower wavenumber means that higher wavenumber eddies (the synoptic scale) will have a suboptimal growth rate. Linear baroclinic theory predicts that the suboptimal baroclinic growth will result in a suboptimal baroclinic structure on average, i.e., with less westward tilt with height, which fits the observed earlier breaking of the baroclinic structure (Figs. 8 and 9), which explains the reduction in eddy strength (Fig. 6b) and lifetime (Fig. 6c).

Intuition to this can be even gained by the simple two-layer baroclinic instability quasigeostrophic (QG) model (Phillips 1954). Phillips shows that for a two-layer model of equal thickness layers, on a beta plane, the wave speed is given by (adopting the notation of Vallis 2006)

$$c = -\frac{1}{K^2 + k_d^2} \left\{ \beta + \frac{\beta k_d^2}{2K^2} \pm \frac{k_d^2}{2K^2} \left[\beta^2 + \frac{4U^2 K^4 (K^4 - k_d^4)}{k_d^4} \right]^{1/2} \right\}, \quad (1)$$

where $K = k^2 + l^2$ is the total wavenumber, β is the planetary vorticity gradient, $U = (U_{\text{up}} - U_{\text{down}})/2$ is half the wind shear, and $k_d = \sqrt{8}/L_d$ is the inverse of the deformation radius:

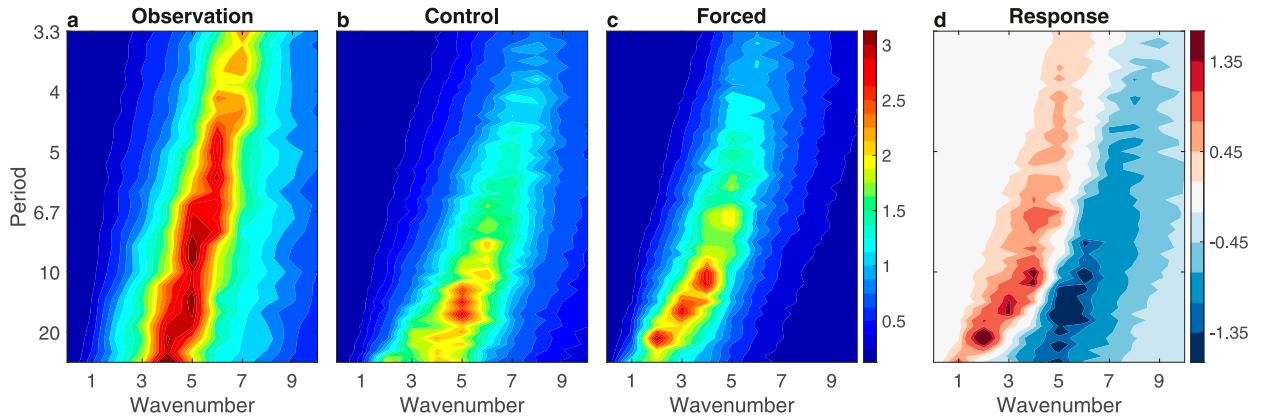


FIG. 10. (a) The vertically integrated momentum, in spectral space, of eastward-propagating waves per volume ($10^4 \times \text{kg m}^{-2} \text{s}^{-1}$), as function of zonal planetary wavenumber ($\sim 5 \times 10^{-8} \text{ m}$) and period (days) of the meridional wind over the midlatitudes for observational data of the Southern Hemisphere during December–February. (b), (c) As in (a), but for data from the control and forced GCM simulation, respectively. (d) The difference between the control and forced simulation. The vertical integration in pressure coordinate is defined as $\bar{P} = \int \bar{v} dp/g$, where \bar{P} and \bar{v} are the meridional momentum and velocity in spectral space. The integration is done from 300 to 850 hPa, and then the momentum is averaged from latitude 30° – 60° . Climatology was removed from the meridional wind to highlight the eddies contribution. Corrections to the wavenumber from the smaller perimeter at high latitudes was neglected. The data for the Earth SH are taken from ERA-Interim.

$$L_D = \frac{NH}{f}, \quad (2)$$

where N is the Brunt–Väisälä frequency, H is the total thickness, and f is the Coriolis parameter. Taking only the imaginary part of Eq. (1) and multiplying by the zonal wavenumber k , we get the growth rate,

$$\sigma = \frac{k}{K^2 + k_d^2} \frac{k_d^2}{2K^2} \left[\frac{4U^2 K^4 (k_d^4 - K^4)}{k_d^4} - \beta^2 \right]^{1/2}. \quad (3)$$

From the plot of the most unstable mode as a function of zonal wavenumber for the control (Fig. 11a, solid) and forced (Fig. 11a, dashed black) simulations based on the mean values that were inferred from the simulation (Table 1), it is apparent that the increase in jet strength and deformation radius indeed shift the energy spectrum toward the planetary scale. The two variables that change significantly are U and N . Accounting only for the jet strengthening significantly increases the maximum growth rate, while shifting it to lower scales (Fig. 11a, dashed blue). When increasing only N , the growth rate also greatly reduces, while also shifting to lower wavenumbers (Fig. 11a, dashed red). Changes in H will produce the same result as it affects the deformation radius in the same way. Studies of the jet strength effect using idealized models, which also incorporate the jet meridional (Harnik and Chang 2004) and vertical (Rivière 2009) structure, and the effect of the atmosphere stratification (Kidston et al. 2010), were conducted in the past, and their results are consistent with the shift observed in our model spectrum.

Repeating the same analysis for the Pacific and Atlantic conditions also requires considering the jet latitude, affecting both the deformation radius (through f) and the β effect (Rivière 2011). In this model's framework, reducing the jet latitude shifts the growth rate to smaller scales and reduces

the maximum growth rate. Plotting the most unstable modes for values assessed over the Pacific (Fig. 11b, solid blue for September–November and dashed blue for December–January) and the Atlantic (Fig. 11b, solid red for September–November and dashed red for December–January) is consistent with why during most seasons there is a midwinter minimum over the Pacific and not over the Atlantic. Over the Pacific, the increase in jet strength is larger, together with an increase in static stability (Frieron and Davis 2011), shifting the growth rate significantly toward the planetary scale, which decrease storm activity. Over the Atlantic, less significant intensification of the jet over the Atlantic and smaller increase in static stability set the overall growth rate in the synoptic scale to be higher. On seasons with a stronger jet over the Atlantic, the shift becomes more significant, and an MWM in the Atlantic storm track is observed (Afargan and Kaspi 2017).

5. Conclusions

In recent years, it has become evident that there is a non-trivial reduction in storm activity during times when the jet is particularly strong. This was first observed over the Pacific Ocean during midwinter (Nakamura 1992) and was further supported by studies of the Atlantic storm track (Afargan and Kaspi 2017) and idealized GCM experiments (Yuval and Kaspi 2016; Yuval et al. 2018; Novak et al. 2020). This evidence seems to contradict the prediction of linear baroclinic instability theory, which has been a key in our understanding of the interaction between the storm tracks and the general circulation, and a fundamental building block of the theoretical understanding of Earth's atmospheric dynamics. Analyzing the phenomenon from an Eulerian perspective is useful, but lacks information about the conditions and evolution that the baroclinic wave undergoes. Therefore, the Lagrangian perspective is complementary in studying the underlying mechanism that

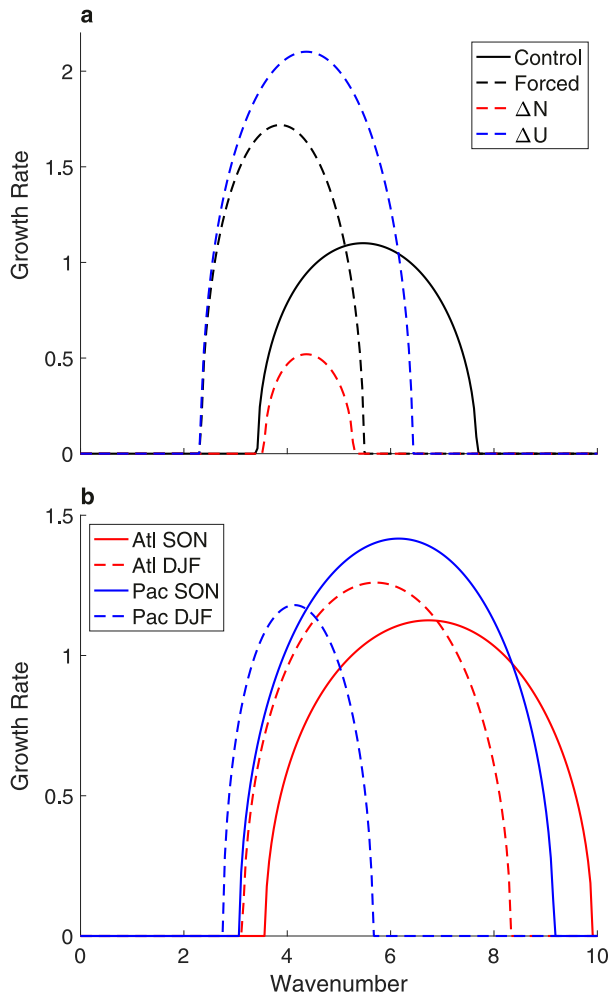


FIG. 11. The growth rate ($\times 10^{-5} \text{ s}^{-1}$) of the QG two-layer model as a function of wavenumber according to Eq. (3). (a) The climatological values from the control (solid black) and forced (dashed black) GCM simulation are substituted into the two-layer growth rate. The response separated to the effect of the change in buoyancy frequency and change in jet intensity are shown in dashed red and blue, respectively. (b) Climatological values of the Atlantic (red) and Pacific (blue) Oceans during September–November (SON; solid) and December–February (DJF; dashed) are used, with the values shown in Table 1.

causes this deviation from linear theory. The Lagrangian approach is even more powerful when performed on idealized GCM data, as it gives a practically limitless amount of data to analyze, while keeping the physical system simple. To study the effect of intense jets on baroclinic eddies, in this study, we analyze a series of idealized GCM simulations with systematically varied jet strengths, from both an Eulerian and Lagrangian perspective. For the Lagrangian analysis, we employ a cyclone tracking algorithm for statistical analysis of the eddy characteristics. The main findings of this study can be summarized as follows:

- A reduction in midlatitude EKE is found in aquaplanet idealized GCM simulations when the subtropical jet is intensified

through strengthening of the Hadley circulation (Figs. 2 and 3).

- Taking a Lagrangian perspective, to address the EKE reduction by following individual storms and analyzing their statistics, three main properties are found to control the eddy activity: the number of storms, their intensity, and their lifetime. Using the tracking data, we assess these properties and their response to the jet intensification.
- Comparing the tracking results between the control and forced simulations (Fig. 6) show that while the eddy intensity does not vary much, the upper-level eddy response is dominated by a change in the number of eddies and, to a lesser extent, by their lifetime. However, the lower-level eddy response is affected jointly by a change in the number of storms and in the eddy lifetime.
- Increasing the jet strength causes a reduction in the pairing between upper- and lower-level eddies and breaks the baroclinic wave (Fig. 8).
- Investigating in detail the vertical structure of the baroclinic wave, we find that jet intensification causes a reduction in the vertical extent of the wave, and faster zonal speed of the higher-level eddies relative to the lower-level eddies, which cause faster dephasing of the baroclinic structure, and thus reducing the lifetime of the baroclinic wave (Fig. 9).
- Overall, the baroclinic wave response to jet intensification causes an early breaking of the baroclinic structure, decreases the vertical extent of the baroclinic wave and reduces the number of waves produced.
- The Lagrangian results are consistent with linear baroclinic instability theory if the energy distribution between scales is considered. An intensified jet shifts the eddy power spectrum from the synoptic scale toward the planetary scale (Fig. 10). The shift means that eddies under these conditions have a suboptimal growth rate, which reduces the amount of baroclinic eddies and explains the decoupling of the baroclinic structure.
- Intuition to the shift and suboptimal growth rate in response to the jet intensification can be gained from the simple two-layer QG model (Phillips 1954). An increase in jet strength and Rossby deformation radius (due to an increase in the buoyancy frequency) shift the growth rate toward lower wavenumbers. Thus, the growth rate of synoptic-scale eddies is suboptimal.
- The two-layer framework with representative parameters for the different storm tracks on Earth supports the simulation results. Over the Pacific, the increase in jet strength during midwinter, together with an increase in static stability (Frierson and Davis 2011), predicts a significant shift toward the planetary scale, which can explain the storm-track observed response. Over the Atlantic, the moderate jet intensification and increase in static stability make the shift marginal, explaining why seasons with strong jets are characterized by a reduction in storm activity (Afargan and Kaspi 2017), while most seasons are not (Fig. 11b). Over the SH storm track, the jet intensification is weaker than over the Pacific, and there is a decrease in static stability. Therefore, as observed, no reduction in EKE during midwinter is expected. It also supports the hypothesis that storm activity over the Atlantic was reduced during the last

TABLE 1. Values substituted in Eq. (3) to plot the curves in Fig. 11. The maximum jet strength is taken as the shear, the latitudinal position of the maximum intensity is used as the latitude in which β and f are calculated, and its height is set as the total thickness; N is taken as the midlatitude value.

	Control	Forced	Atlantic SON	Atlantic DJF	Pacific SON	Pacific DJF
\bar{U} (m s^{-1})	35	75	26	35	35	53
N (10^{-2} s^{-1})	1.2	1.4	1.2	1.25	1.3	1.45
H (km)	10	12	11	12	11	12
Latitude ($^{\circ}$)	30	30	45	42.5	45	32.5

- glacial maximum (Li and Battisti 2008; Löfverström et al. 2016; Rivière et al. 2018).
- By definition, for baroclinic growth, a wind shear is required. On the other hand, per the mechanism presented here, too strong of a shear results in suboptimal baroclinic growth. Thus, there must be a jet velocity that is optimal for eddy growth. Observations indicate that for the Pacific conditions, this value is 45 m s^{-1} (Nakamura 1992).
 - We thus provide a hypothesis for the existence of the MWM in eddy activity over the Pacific.

Acknowledgments. We thank the three reviewers for their helpful comments. This research has been supported by the Israeli Science Foundation under Grant 996/20.

REFERENCES

Afargan, H., 2018: The seasonal cycle of midlatitude storm tracks. Ph.D. thesis, Weizmann Institute of Science, 78 pp.

—, and Y. Kaspi, 2017: A midwinter minimum in Atlantic storm track intensity during years of strong subtropical jet. *Geophys. Res. Lett.*, **44**, 12 511–12 518, <https://doi.org/10.1002/2017GL075136>.

Chang, E. K. M., 2001: GCM and observational diagnoses of the seasonal and interannual variations of the Pacific storm track during the cool season. *J. Atmos. Sci.*, **58**, 1784–1800, [https://doi.org/10.1175/1520-0469\(2001\)058<1784:GAODOT>2.0.CO;2](https://doi.org/10.1175/1520-0469(2001)058<1784:GAODOT>2.0.CO;2).

—, and Y. Guo, 2011: Comments on “The source of the midwinter suppression in storminess over the North Pacific.” *J. Climate*, **24**, 5187–5191, <https://doi.org/10.1175/2011JCLI3987.1>.

Charney, J. G., 1947: The dynamics of long waves in a baroclinic westerly current. *J. Meteor.*, **4**, 136–162, [https://doi.org/10.1175/1520-0469\(1947\)004<0136:TDOLWI>2.0.CO;2](https://doi.org/10.1175/1520-0469(1947)004<0136:TDOLWI>2.0.CO;2).

Christoph, M., U. Ulbrich, and P. Speth, 1997: Midwinter suppression of Northern Hemisphere storm track activity in the real atmosphere and in GCM experiments. *J. Atmos. Sci.*, **54**, 1589–1599, [https://doi.org/10.1175/1520-0469\(1997\)054<1589:MSONHS>2.0.CO;2](https://doi.org/10.1175/1520-0469(1997)054<1589:MSONHS>2.0.CO;2).

Dee, D. P., and Coauthors, 2011: The ERA-Interim reanalysis: Configuration and performance of the data assimilation system. *Quart. J. Roy. Meteor. Soc.*, **137**, 553–597, <https://doi.org/10.1002/qj.828>.

Deng, Y., and M. Mak, 2005: An idealized model study relevant to the dynamics of the midwinter minimum of the Pacific storm track. *J. Atmos. Sci.*, **62**, 1209–1225, <https://doi.org/10.1175/JAS3400.1>.

Eady, E. T., 1949: Long waves and cyclone waves. *Tellus*, **1** (3), 33–52, <https://doi.org/10.3402/tellusa.v1i3.8507>.

Farrell, B. F., and P. J. Ioannou, 1994: A theory for the statistical equilibrium energy spectrum and heat flux produced by transient baroclinic waves. *J. Atmos. Sci.*, **51**, 2685–2698, [https://doi.org/10.1175/1520-0469\(1994\)051<2685:ATFTSE>2.0.CO;2](https://doi.org/10.1175/1520-0469(1994)051<2685:ATFTSE>2.0.CO;2).

Frierson, D. M. W., and N. A. Davis, 2011: The seasonal cycle of midlatitude static stability over land and ocean in global reanalyses. *Geophys. Res. Lett.*, **38**, L13803, <https://doi.org/10.1029/2011GL047747>.

—, I. M. Held, and P. Zurita-Gotor, 2006: A gray-radiation aquaplanet moist GCM. Part I: Static stability and eddy scale. *J. Atmos. Sci.*, **63**, 2548–2566, <https://doi.org/10.1175/JAS3753.1>.

Harnik, N., and E. K. M. Chang, 2004: The effects of variations in jet width on the growth of baroclinic waves: Implications for midwinter Pacific storm track variability. *J. Atmos. Sci.*, **61**, 23–40, [https://doi.org/10.1175/1520-0469\(2004\)061<0023:TEOVII>2.0.CO;2](https://doi.org/10.1175/1520-0469(2004)061<0023:TEOVII>2.0.CO;2).

Hodges, K., 1995: Feature tracking on the unit sphere. *Mon. Wea. Rev.*, **123**, 3458–3465, [https://doi.org/10.1175/1520-0493\(1995\)123<3458:FTOTUS>2.0.CO;2](https://doi.org/10.1175/1520-0493(1995)123<3458:FTOTUS>2.0.CO;2).

James, I. N., 1987: Suppression of baroclinic instability in horizontally sheared flows. *J. Atmos. Sci.*, **44**, 3710–3720, [https://doi.org/10.1175/1520-0469\(1987\)044<3710:SOBIIH>2.0.CO;2](https://doi.org/10.1175/1520-0469(1987)044<3710:SOBIIH>2.0.CO;2).

Kaspi, Y., and T. Schneider, 2011: Downstream self-destruction of storm tracks. *J. Atmos. Sci.*, **68**, 2459–2464, <https://doi.org/10.1175/JAS-D-10-05002.1>.

Kidston, J., S. M. Dean, J. A. Renwick, and G. K. Vallis, 2010: A robust increase in the eddy length scale in the simulation of future climates. *Geophys. Res. Lett.*, **37**, L03806, <https://doi.org/10.1029/2009GL041615>.

Lee, S.-S., J.-Y. Lee, K.-J. Ha, B. Wang, A. Kitoh, Y. Kajikawa, and M. Abe, 2013: Role of the Tibetan Plateau on the annual variation of mean atmospheric circulation and storm-track activity. *J. Climate*, **26**, 5270–5286, <https://doi.org/10.1175/JCLI-D-12-00213.1>.

Li, C., and D. S. Battisti, 2008: Reduced Atlantic storminess during Last Glacial Maximum: Evidence from a coupled climate model. *J. Climate*, **21**, 3561–3579, <https://doi.org/10.1175/2007JCLI2166.1>.

Löfverström, M., R. Caballero, J. Nilsson, and G. Messori, 2016: Stationary wave reflection as a mechanism for zonally zonalizing the Atlantic winter jet at the LGM. *J. Atmos. Sci.*, **73**, 3329–3342, <https://doi.org/10.1175/JAS-D-15-0295.1>.

Nakamura, H., 1992: Midwinter suppression of baroclinic wave activity in the Pacific. *J. Atmos. Sci.*, **49**, 1629–1642, [https://doi.org/10.1175/1520-0469\(1992\)049<1629:MSOBWA>2.0.CO;2](https://doi.org/10.1175/1520-0469(1992)049<1629:MSOBWA>2.0.CO;2).

—, and T. Sampe, 2002: Trapping of synoptic-scale disturbances into the North-Pacific subtropical jet core in midwinter. *Geophys. Res. Lett.*, **29**, 1761, <https://doi.org/10.1029/2002GL015535>.

—, and A. Shimp, 2004: Seasonal variations in the Southern Hemisphere storm tracks and jet streams as revealed in a reanalysis dataset. *J. Climate*, **17**, 1828–1844, [https://doi.org/10.1175/1520-0442\(2004\)017<1828:SVTSH>2.0.CO;2](https://doi.org/10.1175/1520-0442(2004)017<1828:SVTSH>2.0.CO;2).

Novak, L., T. Schneider, and F. Ait-Chaalal, 2020: Midwinter suppression of storm tracks in an idealized zonally symmetric setting. *J. Climate*, **77**, 297–313, <https://doi.org/10.1175/JAS-D-18-0353.1>.

- O’Gorman, P. A., and T. Schneider, 2008a: Energy in midlatitude transient eddies in idealized simulations of changed climates. *J. Climate*, **21**, 5797–5806, <https://doi.org/10.1175/2008JCLI2099.1>.
- , and —, 2008b: The hydrological cycle over a wide range of climates simulated with an idealized GCM. *J. Climate*, **21**, 3815–3832, <https://doi.org/10.1175/2007JCLI2065.1>.
- Park, H., J. C. H. Chiang, and S. Son, 2010: The role of the central Asian mountains on the midwinter suppression of North Pacific storminess. *J. Atmos. Sci.*, **67**, 3706–3720, <https://doi.org/10.1175/2010JAS3349.1>.
- Park, M., and S. Lee, 2020: A mechanism for the midwinter minimum in North Pacific storm-track intensity from a global perspective. *Geophys. Res. Lett.*, **47**, e2019GL086052, <https://doi.org/10.1029/2019GL086052>.
- Pedlosky, J., 1970: Finite-amplitude baroclinic wave. *J. Atmos. Sci.*, **27**, 15–30, [https://doi.org/10.1175/1520-0469\(1970\)027<0015:FABW>2.0.CO;2](https://doi.org/10.1175/1520-0469(1970)027<0015:FABW>2.0.CO;2).
- Penny, S., G. H. Roe, and D. S. Battisti, 2010: The source of the midwinter suppression in storminess over the North Pacific. *J. Climate*, **23**, 634–648, <https://doi.org/10.1175/2009JCLI2904.1>.
- Phillips, N. A., 1954: Energy transformations and meridional circulations associated with simple baroclinic waves in a two level quasi-geostrophic model. *Tellus*, **6**, 273–286, <https://doi.org/10.1111/j.2153-3490.1954.tb01123.x>.
- Rivière, G., 2009: Effect of latitudinal variations in low-level baroclinicity on eddy life cycles and upper-tropospheric wave-breaking processes. *J. Atmos. Sci.*, **66**, 1569–1592, <https://doi.org/10.1175/2008JAS2919.1>.
- , 2011: A dynamical interpretation of the poleward shift of the jet streams in global warming scenarios. *J. Atmos. Sci.*, **68**, 1253–1272, <https://doi.org/10.1175/2011JAS3641.1>.
- , S. Berthou, G. Lapeyre, and M. Kageyama, 2018: On the reduced North Atlantic storminess during the last glacial period: The role of topography in shaping synoptic eddies. *J. Climate*, **31**, 1637–1652, <https://doi.org/10.1175/JCLI-D-17-0247.1>.
- Schemm, S., and T. Schneider, 2018: Eddy lifetime, number, and diffusivity and the suppression of eddy kinetic energy in midwinter. *J. Climate*, **31**, 5649–5665, <https://doi.org/10.1175/JCLI-D-17-0644.1>.
- , and G. Rivière, 2019: On the efficiency of baroclinic eddy growth and how it reduces the North Pacific storm-track intensity in midwinter. *J. Climate*, **32**, 8373–8398, <https://doi.org/10.1175/JCLI-D-19-0115.1>.
- , H. Wernli, and H. Binder, 2021: The storm-track suppression over the western North Pacific from a cyclone life-cycle perspective. *Wea. Climate Dyn.*, **2**, 55–69, <https://doi.org/10.5194/wcd-2-55-2021>.
- Simmons, A. J., and B. J. Hoskins, 1978: The life cycles of some nonlinear baroclinic waves. *J. Atmos. Sci.*, **35**, 414–432, [https://doi.org/10.1175/1520-0469\(1978\)035<0414:TLCOSN>2.0.CO;2](https://doi.org/10.1175/1520-0469(1978)035<0414:TLCOSN>2.0.CO;2).
- Tamarin, T., and Y. Kaspi, 2016: The poleward motion of extratropical cyclones from a potential vorticity tendency analysis. *J. Atmos. Sci.*, **73**, 1687–1707, <https://doi.org/10.1175/JAS-D-15-0168.1>.
- , and —, 2017: Mechanisms controlling the poleward deflection of midlatitude storm tracks. *J. Atmos. Sci.*, **74**, 553–572, <https://doi.org/10.1175/JAS-D-16-0122.1>.
- Tamarin-Brodsky, T., and O. Hadas, 2019: The asymmetry of vertical velocity in current and future climate. *Geophys. Res. Lett.*, **46**, 374–382, <https://doi.org/10.1029/2018GL080363>.
- Vallis, G. K., 2006: *Atmospheric and Oceanic Fluid Dynamics*. Cambridge University Press, 770 pp.
- Wang, J., H.-M. Kim, and E. K. Chang, 2017: Changes in Northern Hemisphere winter storm tracks under the background of Arctic amplification. *J. Climate*, **30**, 3705–3724, <https://doi.org/10.1175/JCLI-D-16-0650.1>.
- Yuval, J., and Y. Kaspi, 2016: Eddy activity sensitivity to changes in the vertical structure of baroclinicity. *J. Atmos. Sci.*, **73**, 1709–1726, <https://doi.org/10.1175/JAS-D-15-0128.1>.
- , H. Afargan, and Y. Kaspi, 2018: The relation between the seasonal changes in jet characteristics and the Pacific midwinter minimum in eddy activity. *Geophys. Res. Lett.*, **45**, 9995–10002, <https://doi.org/10.1029/2018GL078678>.
- Zhang, Y., and I. M. Held, 1999: A linear stochastic model of a GCM’s midlatitude storm tracks. *J. Atmos. Sci.*, **56**, 3416–3435, [https://doi.org/10.1175/1520-0469\(1999\)056<3416:ALSMOA>2.0.CO;2](https://doi.org/10.1175/1520-0469(1999)056<3416:ALSMOA>2.0.CO;2).